Nanobuckling and x-ray photoelectron spectra of carbyne-rich tetrahedral carbon films deposited by femtosecond laser ablation at cryogenic temperatures

A. Hu[a)]
Department of Physics and Astronomy, University of Waterloo, 200 University Ave. West, Waterloo, Ontario, Canada N2L 3G1

S. Griesing
Experimental Physics, Building C 6.3, Universitaet des Saarlandes, P.O. Box 15 11 50, D-66041 Saarbruecken, Germany

M. Rybachuk
Faculty of Built Environment and Engineering, Queensland University of Technology, Gardens Point O 401, GPO Box 2434 Brisbane, Qld 4001 Australia

Q.-B. Lu and W. W. Duley
Department of Physics and Astronomy, University of Waterloo, 200 University Ave. West, Waterloo, Ontario, Canada N2L 3G1

(Received 13 June 2007; accepted 15 August 2007; published online 11 October 2007)

The growth, surface morphology, and electronic binding states of diamondlike films deposited by femtosecond laser ablation on Si wafers at 77 K have been studied in order to elucidate the mechanical properties of this material. Nanoscale buckling has been observed and is found to have a morphology that exhibits a strong dependence on film thickness. Nanobuckling takes the form of quasiperiodic discrete pointlike excursions extending over widths of 50–100 nm. This morphology converts to a regular structure of grooves/ripples with a modulation period of 30–50 nm as the film thickness increases to 300–600 nm. We find that microhardness is not changed in regions where nanobuckling is present. Analysis of Raman and x-ray photoelectron spectra (XPS) demonstrate that nanobuckling can be attributed to the relaxation of internal stress and to the formation of strong C-Si covalent bonds at the C-Si interface. XPS spectra show that the C 1*s* peak is broadened compared to that found in spectra of films deposited using nanosecond laser ablation. This is found to be consistent with a composition that includes *sp*, sp^2, and sp^3-bonded carbon. The unique composition of these films suggests that these materials may find application in electromechanical devices.
 [DOI: 10.1063/1.2786708]

I. INTRODUCTION

The role of internal stress on buckling and delamination of thin films deposited on substrates has been the subject of much interest because of the importance of thin films in industrial products. For example, buckling without delamination of thin metallic films deposited on compliant elastomer substrates can be used to create optical sensors on deformable devices.[1,2] In another application, enhanced field emission has been observed in partially detached diamondlike carbon (DLC) films.[3] It is well known that DLC is an amorphous material with a tetrahedral structure, in which nanoscale sp^2-bonded carbon clusters are embedded in a sp^3-coordinated carbon matrix.[4,5] High internal compressive stresses have been found to be generated in DLC by the surface implantation of energetic carbon ions during deposition.[6] Relief of this internal stress involves buckling and the localized separation of the film from the substrate.[7,8]

On the other hand, DLC films deposited using femtosecond pulsed laser ablation (fs-DLC) exhibit low stress despite the fact that carbon ion energies are often in the keV range.[9,10] Low compressive stress in these materials is evidently due to the annealing during high energy ion impact.[11] This effect is not observed in DLC films deposited using nanosecond laser ablation (ns-DLC), where the ion energy is $\leq$10 eV. This difference may be due, in part, to the relatively low fraction of sp^3-bonded carbon in fs-DLC deposited at room temperature (0.4–0.6) compared to that in ns-DLC ($\approx$0.7).[12] It has been shown that a fs-DLC film deposited at room temperature possesses a mixture of *sp*-, sp^2-, and sp^3-coordinated carbon.[12] Since *sp*-bonded carbon chains are linear molecular conductors and have been shown to be the precursors of nanotubes,[13] it is of interest to study the microstructure and electron bonding states in fs-DLC films deposited at cryogenic temperatures.

In this work, we report the observation of a nanobuckling structure in fs-DLC deposited on Si. The occurrence and evolution of this structure have been investigated using atomic force microscopy (AFM) analysis as well as by Raman and x-ray photoelectron spectroscopy (XPS). The mechanical properties of these materials have also been characterized using nanoindentation techniques. These measurements are shown to reveal insight into the origin of nanobuckling in DLC materials as well as the role played by the presence of sp/sp^2 clusters.

[a)]Electronic mail: a2hu@uwaterloo.ca

II. EXPERIMENTAL DETAILS

Amorphous carbon thin films were deposited on polished *p*-type Si wafers with (100) orientation. Before deposition, the Si wafer was first degreased in an ultrasonic bath of acetone (high-performance liquid chromatography grade), and then further cleaned by immersion in a 1% HCl solution. The wafer was then rinsed in nanopure water (18 MΩ). The Si wafer was cooled to 77 K by liquid nitrogen in a high-vacuum deposition chamber at a base pressure of 2×10^{-7} Torr (2.67×10^{-5} Pa) evacuated with a turbomolecular pump. During deposition the pressure typically increased to 5×10^{-7} Torr. A regenerative Ti:sapphire laser system ($\lambda=800$ nm, pulse duration $\tau=120$ fs, repetition frequency 500 Hz, incidence angle 45°) was employed to ablate high purity pyrolytic graphite (99.99%). The laser beam was focused into a spot with a typical size of 100 μm by a quartz lens with a focal length of 160 mm. The fs pulse energy was 1 mJ and the peak laser intensity was 1.1×10^{14} W/cm^2 corresponding to a fluence of 12.7 J/cm^2 at the target surface. Details on the deposition system with the ns laser source have been reported elsewhere.[4,5]

Film thickness was monitored *in situ* by measuring the UV absorption of the sample during deposition. The final thickness was measured with a profilometer (AMBios XP-2) after deposition. Microstructure was characterized via scanning electron microscopy (SEM) equipped with a field emission gun and AFM. The microhardness and reduced elastic modulus were determined from load-displacement curves obtained using a Nano Indenter (Hysitron) apparatus. A three-sided pyramid Berkovich indenter was used in the experiment.

UV Raman spectra were obtained with a Kimmon 5161R-GS Raman spectrometer using He/Cd laser radiation at 325 nm (UV, 3.8 eV). To avoid excessive heating of the carbon sample, the laser power was reduced to 4.5 mW. Visual Raman spectra were measured using a Renishaw micro-Raman spectrometer with a 0.3–3 mW He-Ne laser at an excitation wavelength of 632 nm (1.97 eV). For both spectrometers the resolution was 1 cm^{-1}. XPS measurements were carried out using a multitechnique ultrahigh vacuum imaging XPS microprobe spectrometer (Thermo VG Scientific ESCALab 250) with a monochromatic Al $K\alpha$ 1486.6 eV x-ray source. The spectrometer was calibrated by Au $4f_{7/2}$ (binding energy of 84.0 eV) with respect to the Fermi level. The chamber vacuum level was maintained below 2×10^{-10} Torr. The constant pass energy was set at 160 eV for survey scans at 1 eV step and 100 ms per scan. Only one scan was used to collect the spectra. The pass energy of 20 eV was used for C 1*s*/O 1*s*/Si 2*p* scans, with an energy resolution of 0.05 eV. The dwell time was 250 ms and three sweeps were used. Films with 300 nm were used for the survey scanning and the C 1*s* line study while a 40 nm thin film was employed for the Si 2*p* and O 1*s* line scanning in order to focus on binding properties of film-Si substrate interfaces.

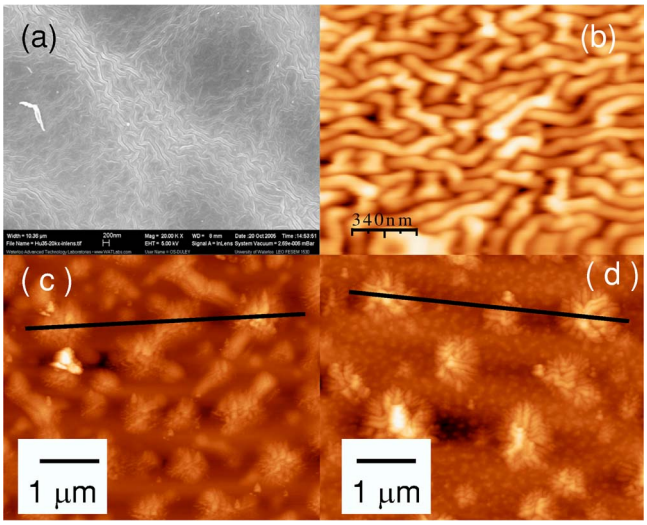

FIG. 1. (Color online) Morphology of diamondlike carbon films deposited by fs laser deposition at 77 K. (a) SEM image of a film with 600 nm thickness (sample A), (b) AFM micrograph of sample A, (c) SEM image of a film with 450 nm thickness (sample B), and (d) SEM image of a film with 300 nm thickness (sample C).

III. RESULTS

A. Nanostructure and nanobuckling

Figure 1 shows the nanostructure observed in fs-DLC films deposited on Si at 77 K as a function of deposition time. The morphology of films after a 7 min deposition (sample A) is shown in Figs. 1(a) and 1(b). Figures 1(c) and 1(d) (samples B and C, respectively) were deposited for 5 and 3 min, respectively. The film thickness for samples A and C as measured with a profilometer is shown in Fig. 2(a). The sharp step in Fig. 2(a) occurs along the line where the substrate was masked prior to deposition. Surface roughness along the straight lines appearing in Figs. 1(c) and 1(d) is recorded in Fig. 2(b). These measurements show that surface buckling develops as the film thickness increases. At a thickness of 300 nm (sample C), peeling occurs at intervals of ≈1.5 μm in the form of pointlike buckling sites having dimensions of ≈1 μm. The amplitude of height modulation in these regions is ≈20 nm. The regions of the film between the sites of pointlike buckling appear granular, i.e., consist of a matrix assembled from nanoclusters.

As the thickness increases to 450 nm (sample B) the buckling amplitude increases to ≈60 nm [Fig. 2(b)] and surface peeling develops a linear structure with segments oriented approximately perpendicular to each other. The resulting ripples can be clearly seen in Fig. 1(c). With a further increase in film thickness to 600 nm [Figs. 1(a) and 1(b)], these ripples increase in amplitude and are separated by ≈100 nm. Each ripple extends over a length of $\approx500-3000$ nm and the pattern, as a whole, is found to cover the entire surface of the sample. The morphology observed in fs-DLC samples is quite different from that seen in DLC films, where partial detachment of films occurs on a scale of micrometers and there is no substructure in the detached regions.[3,7,8]

To explore the origin of nanobuckling in fs-DLC, we further investigate films with a smaller thickness and exam-

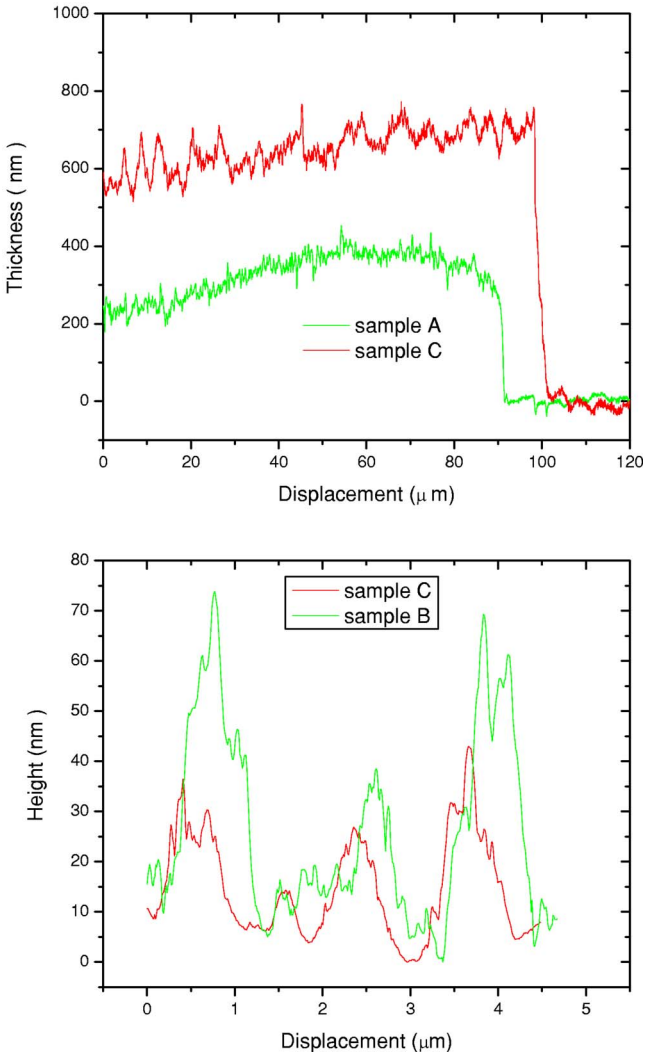

FIG. 2. (Color online) (a) Film thickness as measured using a profilometer. (b) Surface roughness analysis along the straight lines shown in Figs. 1(c) and 1(d).

ine the effect of thermal processing on these samples. Figures 3(a) and 3(b) shows the microstructure of a 50 nm thick film (sample D) after deposition for 1 min. Figures 3(c) and 3(d) are micrographs of thick sample B [as initially shown in Fig. 1(c)] after temperature cycling between 77 and 300 K. This cycle involved taking a sample deposited at 77 K to 300 K for 1/2 h and keeping it there for 30 min, and then recooling it to 77 K before the final observation at 300 K. The same rate is employed for warning up and cooling down. This cycle was carried out in vacuum in order to avoid the influence of moisture. Figures 3(a) and 3(b) display the buckling that appears in the 50 nm film, which is representative of the initial growth stage. The inset in Fig. 3(a) shows that buckling takes the form of a grouping of discrete dots in some locations. These subsequently join up to form the stripes that are evident in Fig. 3(b).

Figure 3(c) shows the micron-scale buckling formed by thermal cycling in a 300 nm thick fs-DLC film (sample E). The local morphology at one buckling site is shown at higher magnification in Fig. 3(d). This type of buckling also appears in thick ns-DLC films, and likely originates from thermally

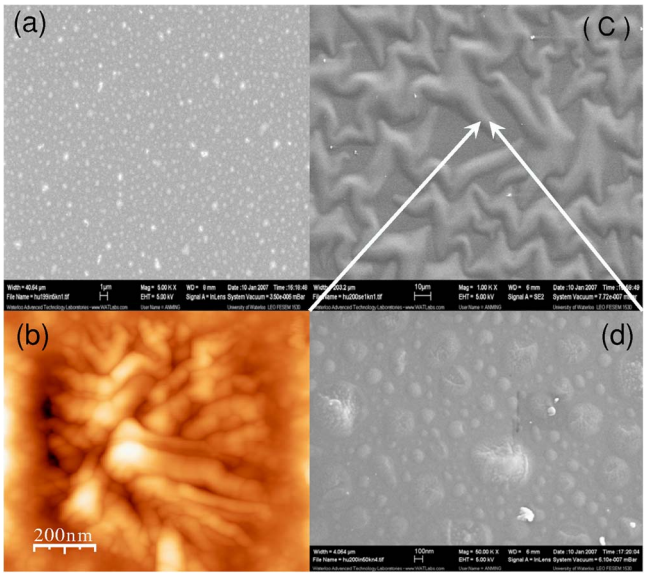

FIG. 3. (Color online) (a) SEM image and (b) AFM micrograph of fs-DLC films deposited for 1 min with a thickness of 50 nm (sample D). (c) SEM image of fs-DLC films with of a thickness of 300 nm after thermal processing (sample E). (d) A magnified SEM image corresponding to a point located on a buckling branch as indicated in (c). The white arrow points to the position observed in a high resolution.

induced stress relief.[3,7,8] It is necessary to mention that the present temperature increasing/decreasing rate is the biggest value we can employ. With a slower rate, such as a thermal cycling in 2 h, the microbuckling almost disappears. Hence, the present results show that nanoscale buckling created during deposition and micron-scale buckling generated by thermal stress can coexist in fs-DLC films deposited at cryogenic temperatures.

B. Internal stress and nanohardness

Figure 4 shows Raman spectra of two fs-DLC films deposited at 77 K recorded with 628 nm excitation. The broad asymmetric band at 1100–1700 cm^{-1} corresponds to the overlapped *D* and *G* bands of tetrahedral carbon. The *D* and *G* bands, centered at 1355 cm^{-1} and 1570 cm^{-1}, respec-

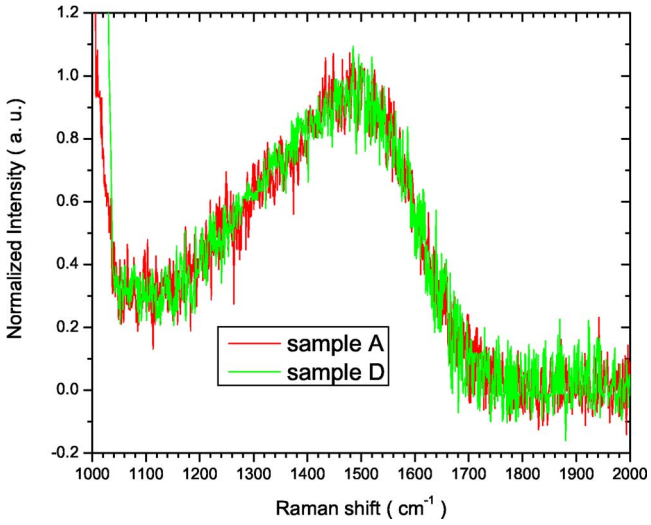

FIG. 4. (Color online) Raman spectra recorded at 632 nm for fs-DLC films.

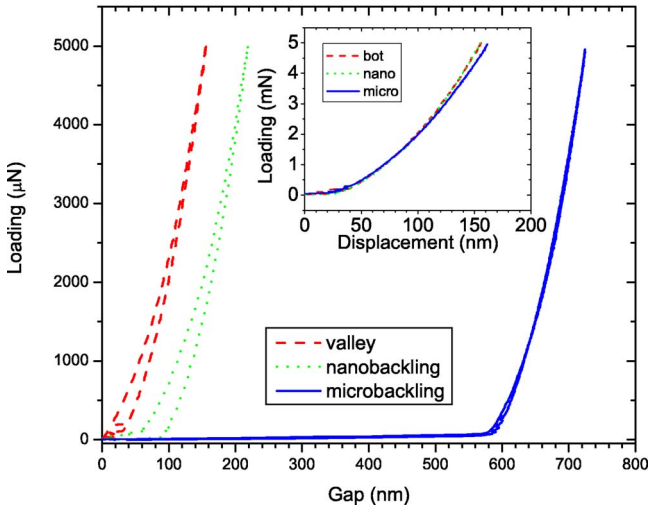

FIG. 5. (Color online) Load-displacement curves measured by a nanoindenter at different positions of sample E.

tively, arise from the stretching and breathing modes of sp^2-bonded carbon.[14] As a result, the relative concentration of sp^3-bonded species can be estimated by deconvolving the D/G band into the two components.[4,5,14] Such an analysis shows that the fraction of sp^3-bonded carbon in these materials is ≈0.55.[12] As the D/G band is sensitive to internal stress and shifts to higher frequency with increasing stress, the Raman spectrum can be used to map this effect.[15,16] Spectra in Fig. 4 then show that the D/G band of fs-DLC is independent of thickness, indicating that both internal stress and the concentration of sp^3-bonded carbon are not functions of film thickness.

Figure 5 demonstrates three loading-displacement curves measured at different positions of sample E by a nanoindenter with a 5 μN force. The plot designated as "microbuckling" is obtained at a peak of the microbuckling pattern. The "nanobuckling" plot was measured in the valley of the microbuckling pattern, but on top of a nanobuckling feature. The "valley" line corresponds to a measured point at a point on the surface without any buckling. Values of the nanohardness, reduced elastic modulus, and contact stiffness can be obtained by fits to free-load drawback curves.[17] By fitting to the valley curve, a hardness of 16.7 GPa and a reduced modulus of 177 GPa are found in nonbuckling areas. These values are slightly lower than those measured for fs-DLC deposited at room temperature, where the sp^3-bonded carbon fraction is 0.7.[11]

The curves measured on the top of both microbuckling and nanobuckling features show unsupported displacements of 580 and 60 nm, respectively. From the roughness analysis shown in Fig. 1 it is reasonable to conclude that this initial free-loading displacement is a consequence of partial detachment of the films from the substrate. The load-displacement curves have been replotted in the inset in Fig. 5 after removal of the displacement at a force of 2 μN, and it evident that valley and nanobuckling curves then coincide. This indicates that the mechanical properties are unchanged in both micro- and nanobuckling regions. However, microbuckling shows a slightly larger displacement at a given loading than is seen in the other two locations. This may signal a higher concentration of defects in this region, leading to reduced hardness.

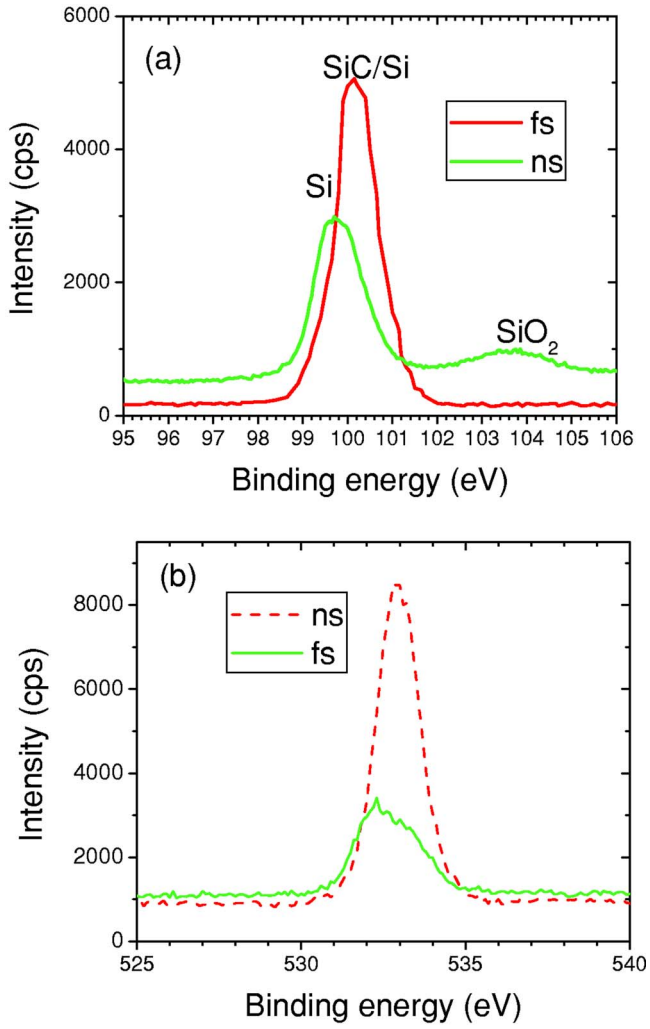

FIG. 6. (Color online) (a). Si 2p core-level XPS spectra for fs-DLC and ns-DLC samples (both 40 nm in thickness) deposited at 77 K. (b) O 1s core-level binding energy for fs-DLC and ns-DLC samples (both 40 nm in thickness) deposited at 77 K.

C. XPS spectra

To examine the influence of interfaces between the carbon film and Si substrate on nanostructure, XPS spectra of fs-DLC and ns-DLC films deposited at 77 K, both with a thickness of about 40 nm, are compared in Fig. 6. Figure 6(a) shows spectra of fs-DLC and ns-DLC films in the region of the Si 2p core energy level. Three distinct valence states of Si are detected, one located at 99.6 eV, the second at 100.2 eV, and the third at 103.6 eV. The peak at 99.6 eV can be attributed to the Si substrate and 100.2 eV is identified with the charge neutral covalent state in SiC, while that at 103.6 eV arises from the +4 oxidation state in SiO_2.[18–22] To obtain a detailed deconvolution of Si 2p one has to consider the split of Si 2p and low-shifting of Si 2p by the screening of a covalent state. However, it is evident that the Si 2p peak of fs-DLC films is at an intensity approximately twice that of the peak seen in ns-DLC films. As a result, it is apparent that SiC is preferentially formed at the C-Si interface in fs-DLC.

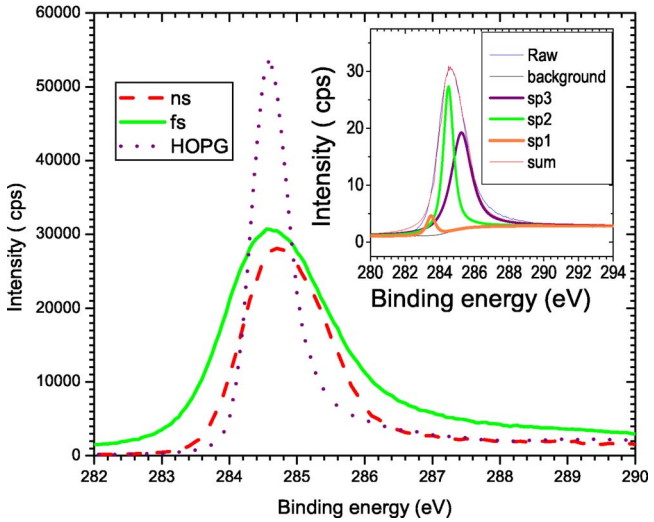

FIG. 7. (Color online) XPS spectra for the C 1*s* core-level binding energy for fs-DLC (300 nm in thickness), ns-DLC (300 nm in thickness), and HOPG samples.

The passivating SiO_2 layer present on Si is absent in fs-DLC, but is found in ns-DLC films. This effect can be also seen in Fig. 6(b), which shows spectra of the O 1*s* core energy level in fs- and ns-DLC films. The intensity of the O 1*s* level in ns-DLC is roughly three times that in fs-DLC, indicating that a SiO_2 layer is attached to the substrate surface in ns-DLC but has been partially removed in fs-DLC films.

The origin of this SiO_2 layer is uncertain since cleaning in dilute HCl will remove the majority of the original SiO layer on the Si wafer and inhibit further oxidation by dangling Si bonds with H atoms. However, after deposition at cryogenic temperatures, ns-DLC graphitizes on a submicron scale and exhibits an enhanced affinity for oxygen.[5] The diffusion of oxygen may then further oxidize the Si surface. As a similar graphitization does not occur in fs-DLC, this may account for the presence of SiO_2 in ns-DLC and not in fs-DLC, which only shows a preferential SiC layer. It is also possible that the high energy ions in fs ablation can remove any residual SiO_2 at the Si surface. This model would be consistent with the observed low abundance of SiO_2 in ns-DLC deposited at room temperature.[5] The thickness of the SiC layer is worth further investigation.

XPS spectra of fs-DLC, ns-DLC, and a highly oriented pyrolytic graphite (HOPG) sample in the C 1*s* region are shown in Fig. 7. The fs-DLC and ns-DLC films were both deposited at 77 K with a thickness of 300 nm. In these spectra, the C 1*s* peak in fs-DLC has a full width at half height (FWHH) of 1.9 eV while the FWHH in ns-DLC is 1.5 eV. The C 1*s* peak in HOPG has a FWHH of 0.7 eV. Deconvolution of the broad C 1*s* core-level peak into sp^2-bonded carbon (at 284.4 eV) and sp^3-bonded carbon (at 285.2 eV) components in ns-DLC can be used to show that the sp^2 content in these films is 0.68.[4,23,24] The C 1*s* peak of carbyne (*sp*-bonded carbon chains) is found at 283.5 eV, a lower level.[25,26] Hence, the broad C 1*s* peak in fs-DLC, which includes an additional component near 284 eV, indicates that these films contain *sp*-bonded as well as sp^2- and sp^3-bonded species. Based on a mixture of sp^1(283.5 eV)-, sp^2(284.4 eV)-, and sp^3(285.2 eV)-bonded components, a deconvolution of C 1*s* line of fs-DLC is shown in the inset to Fig. 7. The concentrations of three bonded carbons in cryogenic fs-DLC are obtained as $0.05(sp^1)$, $0.4(sp^2)$, and $0.55(sp^3)$, consistent with the quantitative analysis of UV-vis Raman spectra, which has a slightly higher sp^3 content (0.51 in fs-DLC deposited in room temperature).[12]

IV. DISCUSSION

It is well established that buckling originates in response to stress relief and that the resulting profile of the surface is governed by the distribution of internal stress. These quantities reflect the value of Young's modulus as well as the adhesion energy at the film-substrate interface.[7,8,27] Furthermore, enhanced bonding between the film and substrate in fs-DLC is evident from XPS spectra, which show the formation of Si–C covalent bonds at the interface. These bonds are less apparent in the spectra of ns-DLC. As a result, one expects a higher adhesion energy in fs-DLC than in ns-DLC films. From Matuda,[27] the adhesion energy, U_a, as a function of buckling width is $U_a=[c^2\pi^2Ed^3/12(1-v^2)][L/l^2(L-l)]$, where E is Young's modulus, v is the Poisson ratio, d is the film thickness, L isthe width of the whole film, c is a constant, and l is the buckling wavelength. Then, as U_a increases, l will generally decrease. This connection between buckling width and adhesion energy explains why nanobuckling is observed in fs-DLC and not in ns-DLC films. One can also see that as d increases, l will also increase if U_a is constant. This correlation is also evident in Fig. 1. Since the energy of C ions in fs ablation is 1–2 keV, compared to $\leq$10 eV in ns-DLC,[9,10,28] C ions can directly implant into the substrate surface, forming covalent Si–C bonds. This may explain why nanobuckling is absent in ns-DLC films deposited at cryogenic temperatures.[5] Other solutions of the buckling equation based on a thin shell model predict pointlike, flower shaped, and wavy relief patterns.[7,8] This may account for pointlike and stripelike patterns observed in fs-DLC, although further analysis of these effects is required for nanoscale buckled structures.

Surface charging in XPS samples results in shifting of peaks to higher energy. Hence, the redshift of the C 1*s* peak in fs-DLC (Fig. 7) cannot be attributed to surface charging. The presence of *sp*-bonded carbon chains in fs-DLC would be in keeping with the shift of the C 1*s* level to lower energy, as seen in Fig. 7. Then it can be concluded that fs-DLC films can be regarded as constituting a novel carbonaceous material with mixed $sp/sp^2/sp^3$ bonding. The data discussed here show that the inclusion of *sp*-bonded carbon does not dramatically modify the mechanical properties of DLC. However, unlike semiconducting/insulating ns-DLC, the present fs-DLC films are conducting. Due to the enhanced stability of *sp*-bonded carbon chains in the present composition we assume they are terminated by graphite clusters.[29] Because *sp*-bonded carbon chains are molecular conductors, the conductivity of fs-DLC films can be enhanced by a percolation network, i.e., bridging sp^2 clusters by *sp*-bonded carbon chains although the sp^1 concentration is still low. The microstructure and mechanical properties of nanobuckled fs-DLC

films then make this material a promising candidate for field emission sources or as an element in electromechanical devices since the buckling significantly changes the transporting properties.[1–3] A special application is a pressure sensor sampling a nanoscopic displacement. Due to the high hardness of nanobuckling of fs-DLC, such a sensor is expected to work on a high pressure range than that of microbuckling metallic films on elastomer substrates.

V. CONCLUSIONS

The presence of microstructure and nanobuckling in fs-DLC films deposited at 77 K has been investigated. A nanobuckling structure has been found to be a function of film thickness and is shown to arise from enhanced film-substrate adhesion energy. This occurs as the result of the formation of C–Si covalent bonds as high energy C ions impact on the Si surface during the initial stages of deposition. Our analysis indicates that these materials have mixed $sp/sp^2/sp^3$ bonding. This may make these materials of interest in applications.

ACKNOWLEDGMENT

This work was supported by a grant from the Natural Science and Engineering Research Council of Canada (NSERC).

[1]N. Bowden, S. Brittain, A. G. Evans, J. W. Hutchinson, and G. M. Whitesides, Nature (London) **393**, 146 (1998).
[2]S. P. Lacour, S. Wagner, Z. Huang, and Z. Suo, Appl. Phys. Lett. **82**, 2404 (2003).
[3]T. Tharigen, E. Hartmann, M. Lenk, A. Mende, K. Otte, M. Lorenz, and K. H. Hallmeier, Appl. Surf. Sci. **182**, 142 (2001).
[4]A. Hu, I. Alkhesho, H. Zhou, and W. W. Duley, Diamond Relat. Mater. **16**, 149 (2007).
[5]A. Hu, I. Alkhesho, W. W. Duley, and H. Zhou, J. Appl. Phys. **100**, 084319 (2006).
[6]D. R. McKenzie, D. Muller, and B. A. Pailthorpe, Phys. Rev. Lett. **67**, 773 (1991).
[7]D. Nir, Thin Solid Films **112**, 41 (1984).
[8]S. B. Iyer, K. S. Harshavardhan, and V. Kumar, Thin Solid Films **256**, 94 (1995).
[9]P. S. Banks, L. Dinh, B. C. Stuart, A. M. Komashko, A. M. Rubenchik, M. D. Perry, and W. McLean, Appl. Phys. A **69**, S347 (1999).
[10]F. Qian, V. Craciun, R. K. Singh, S. D. Dutta, and P. P. Pronko, J. Appl. Phys. **86**, 2281 (1999).
[11]F. Garrelie, A. S. Loir, C. Donnet, F. Rogemond, R. Le Harzic, M. Belin, E. Audouard, and P. Laporte, Surf. Coat. Technol. **163–164**, 306 (2003).
[12]A. Hu, Q. B. Lu, W. W. Duley, and M. Rybachuk, J. Phys. Chem. **126**, 154705 (2007).
[13]L. Ravagnan, F. Siviero, C. Lenardi, P. Piseri, E. Barborini, and P. Milani, Phys. Rev. Lett. **89**, 285506 (2002).
[14]A. C. Ferrari and J. Robertson, Phys. Rev. B **61**, 14095 (2000).
[15]J. W. Ager III, S. Anders, A. Anders, and I. G. Brown, Appl. Phys. Lett. **66**, 3444 (1995).
[16]A. C. Ferrari, B. Kleinsorge, N. A. Morrison, A. Hart, V. Stolojan, and J. Robertson, J. Appl. Phys. **85**, 7191 (1999).
[17]J. Robertson, Mater. Sci. Eng., B **37**, 129 (2002).
[18]XPS data bank at http://srdata.nist.gov/xps/
[19]S. V. Didziulis and P. D. Fleischauer, Langmuir **6**, 621 (1990).
[20]M. A. Hartney, J. N. Chiang, D. W. Hess, and D. S. Soane, Appl. Phys. Lett. **54**, 1510 (1989).
[21]K. L. Smith and K. M. Black, J. Vac. Sci. Technol. A **2**, 744 (1984).
[22]G. G. Jernigan, R. E. Stahlbush, and N. S. Saks, Appl. Phys. Lett. **77**, 1437 (2000).
[23]J. Diaz, G. Paolicelli, S. Ferrer, and F. Comin, Phys. Rev. B **54**, 8064 (1996).
[24]R. Haerle, E. Riedo, A. Pasquarello, and A. Baldereschi, Phys. Rev. B **65**, 045101 (2001).
[25]L. Zhang, H. Ma, N. Yao, Z. Lu, and B. Zhang, J. Vac. Sci. Technol. B **25**, 545 (2007).
[26]I. P. Sergushin, Yu. P. Kudryavtsev, V. M. Elizen, A. P. Sadovskii, A. M. Sladkov, V. I. Nefedov, and V. V. Korshak, J. Struct. Chem. **18**, 553 (1978).
[27]N. Matuda, S. Baba, and A. Kinbara, Thin Solid Films **81**, 301 (1981).
[28]W. W. Duley, *UV Lasers: Effects & Applications in Materials Science* (Cambridge University Press, Cambridge, 1996), Chap. 9, pp. 367–376.
[29]A. Hu, I. Alkhesho, and W. W. Duley, Astrophys. J. **653**, L157 (2006).